

AD 732856

Microwave Breakdown on a Symmetrically Excited Conical Reentry Vehicle

Prepared by K. M. SOOHOO and G. C. LIGHT
Plasma Research Laboratory
and
J. E. TROUSDALE
Avco Corporation

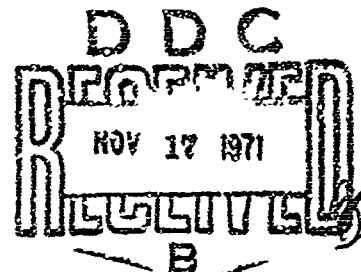
71 OCT 01

Laboratory Operations
THE AEROSPACE CORPORATION

Prepared for SPACE AND MISSILE SYSTEMS ORGANIZATION
AIR FORCE SYSTEMS COMMAND
LOS ANGELES AIR FORCE STATION
Los Angeles, California

Reproduced by
NATIONAL TECHNICAL
INFORMATION SERVICE
Springfield, Va. 22151

APPROVED FOR PUBLIC RELEASE:
DISTRIBUTION UNLIMITED



Air Force Report No.
SAMSO-TR-71-229

Aerospace Report No.
TR-0172(2220-10)-1

MICROWAVE BREAKDOWN ON A SYMMETRICALLY
EXCITED CONICAL REENTRY VEHICLE

Prepared by

K. M. SooHoo and G. C. Light
Plasma Research Laboratory

and

J. E. Trousdale
Avco Corporation

71 OCT 01

Laboratory Operations
THE AEROSPACE CORPORATION

Prepared for

SPACE AND MISSILE SYSTEMS ORGANIZATION
AIR FORCE SYSTEMS COMMAND
LOS ANGELES AIR FORCE STATION
Los Angeles, California

Approved for public release; distribution unlimited

LABORATORY OPERATIONS

The Laboratory Operations of The Aerospace Corporation is conducting experimental and theoretical investigations necessary for the evaluation and application of scientific advances to new military concepts and systems. Versatility and flexibility have been developed to a high degree by the laboratory personnel in dealing with the many problems encountered in the nation's rapidly developing space and missile systems. Expertise in the latest scientific developments is vital to the accomplishment of tasks related to these problems. The laboratories that contribute to this research are:

Aerodynamics and Propulsion Research Laboratory: Launch and reentry aerodynamics, heat transfer, reentry physics, propulsion, high-temperature chemistry and chemical kinetics, structural mechanics, flight dynamics, atmospheric pollution, and high-power gas lasers.

Electronics Research Laboratory: Generation, transmission, detection, and processing of electromagnetic radiation in the terrestrial and space environments, with emphasis on the millimeter-wave, infrared, and visible portions of the spectrum; design and fabrication of antennas, complex optical systems, and photolithographic solid-state devices; test and development of practical superconducting detectors and laser devices and technology, including high-power lasers, atmospheric pollution, and biomedical problems.

Materials Sciences Laboratory: Development of new materials; metal matrix composites and new forms of carbon; test and evaluation of graphite and ceramics in reentry; spacecraft materials and components in radiation and high-vacuum environments; application of fracture mechanics to stress corrosion and fatigue-induced fractures in structural metals; effect of nature of material surfaces on lubrication, photosensitization, and catalytic reactions; and development of prosthesis devices.

Plasma Research Laboratory: Reentry physics and nuclear weapon effects; the interaction of antennas with reentry plasma sheaths; experimentation with thermonuclear plasmas; the generation and propagation of plasma waves in the magnetosphere; chemical reactions of vibrationally excited species in rocket plumes; and high-precision laser ranging.

Space Physics Laboratory: Aeronomy; density and composition of the atmosphere at all altitudes; atmospheric reactions and atmospheric optics; pollution of the environment; the sun, earth's resources; meteorological measurements; radiation belts and cosmic rays; and the effects of nuclear explosions, magnetic storms, and solar radiation on the atmosphere.

THE AEROSPACE CORPORATION
El Segundo, California

ACQUISITION NO.		
CFSTI	WHITE SECTION <input checked="" type="checkbox"/>	
DDC	DIFF. SECTION <input type="checkbox"/>	
UNCLASSIFIED	<input type="checkbox"/>	
JUSTIFICATION		
BY		
DISTRIBUTION/AVAILABILITY CODES		
DIST.	AVAIL. AND/OR	SPECIAL
A		

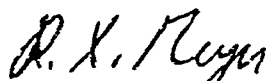
FOREWORD

This report is published by The Aerospace Corporation, El Segundo, California, under Air Force Contract No. F04701-71-C-0172.

This report, which documents research carried out from June 1970 through April 1971, was submitted to Capt. Richard K. Strome, SYAE, on 26 July 1971 for review and approval.

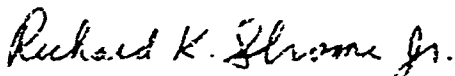
The authors thank R. M. Glasser for his help in obtaining and evaluating the experiment data.

Approved



R. X. Meyer, Director
Plasma Research Laboratory

Publication of this report does not constitute Air Force approval of the report's findings or conclusions. It is published only for the exchange and stimulation of ideas.



Richard K. Strome, Jr., Capt., USAF
Project Officer

UNCLASSIFIED
Security Classification

DOCUMENT CONTROL DATA - R & D		
<i>(Security classification of title, body of abstract and indexing annotation must be entered when the overall report is classified)</i>		
1. ORIGINATING ACTIVITY (Corporate author) The Aerospace Corporation El Segundo, California		2a. REPORT SECURITY CLASSIFICATION Unclassified
2b. GROUP		
3. REPORT TITLE Microwave Breakdown on a Symmetrically Excited Conical Reentry Vehicle		
4. DESCRIPTIVE NOTES (Type of report and inclusive dates)		
5. AUTHOR(S) (First name, middle initial, last name) Keith M. SouHoo, Glenn C. Light, and John E. Trousdale		
6. REPORT DATE 71 OCT 01	7a. TOTAL NO. OF PAGES 37	7b. NO. OF REFS 14
8a. CONTRACT OR GRANT NO. F04701-71-C-0172	9a. ORIGINATOR'S REPORT NUMBER(S) TR-0172(2220-10)-1	
b. PROJECT NO.	9b. OTHER REPORT NO(S) (Any other numbers that may be assigned this report) SAMSO-TR-71-229	
c.		
d.		
10. DISTRIBUTION STATEMENT Approved for public release; distribution unlimited		
11. SUPPLEMENTARY NOTES	12. SPONSORING MILITARY ACTIVITY Space and Missile Systems Organization Air Force Systems Command Los Angeles, California	
13. ABSTRACT Predictions and measurements of microwave breakdown in air are compared for a conical reentry vehicle model with an overall length of approximately one wavelength. The vehicle is excited by means of a circumferential gap to form an asymmetric dipole with roll-symmetric radiation. Measurements performed in an evacuable chamber show breakdown occurring at either the nose tip or the feed gap, or simultaneously in both regions, depending upon the gas pressure. The electric fields are computed as functions of distance radially from the nose tip and normally from the feed gap by the use of moment methods. The breakdown calculation is based on a variational technique that can accommodate cw or pulsed breakdown and can handle nonuniformities in both gas properties and electric fields. Breakdown behavior is calculated at the nose tip and at the feed gap. Theory and experiment are shown to agree within the estimated accuracy of the experiment.		

DD FORM 1473

UNCLASSIFIED
Security Classification

ABSTRACT

Predictions and measurements of microwave breakdown in air are compared for a conical reentry vehicle model with an overall length of approximately one wavelength. The vehicle is excited by means of a circumferential gap to form an asymmetric dipole with roll-symmetric radiation. Measurements performed in an evacuable chamber show breakdown occurring at either the nose tip or the feed gap, or simultaneously in both regions, depending upon the gas pressure. The electric fields are computed as functions of distance radially from the nose tip and normally from the feed gap by the use of moment methods. The breakdown calculation is based on a variational technique that can accommodate cw or pulsed breakdown and can handle nonuniformities in both gas properties and electric fields. Breakdown behavior is calculated at the nose tip and at the feed gap. Theory and experiment are shown to agree within the estimated accuracy of the experiment.

KEY WORDS

**Conical reentry vehicle
Gap breakdown
Gap-fed conical antenna
Input admittance
Microwave breakdown
Nose-tip breakdown
Nonuniform near fields**

Distribution Statement (Continued)

Abstract (Continued)

CONTENTS

FOREWORD	ii
ABSTRACT	iii
I. INTRODUCTION	1
II. DESCRIPTION OF EXPERIMENTAL MODEL	3
III. NEAR-FIELD CALCULATIONS	5
IV. BREAKDOWN CALCULATIONS	15
V. EXPERIMENT AND RESULTS	23
VI. DISCUSSION.	31
REFERENCES	33

FIGURES

1. Model Circumferential Gap Antenna	4
2. Theoretical Cone Model	6
3. Total Current Distribution Along Generating Arc	9
4. Calculated and Measured Directivity Patterns	10
5. Near-Field Distributions at Gap and Tip for Frequency = 1500 MHz and Gap Height = 0.1 in.	12
6. Near-Field Distributions at Gap and Tip for Frequency = 1560 MHz and Gap Height = 0.2 in.	13
7. Calculated Diffusion Length	20
8. Test for Validity of CW Breakdown Assumption Ratio in Finite Time to Diffusion Time	21
9. Power Breakdown Test Instrumentation	24

10.	Calculated Gap Breakdown Compared with Experimental Data for Frequency = 1500 MHz and Gap Height = 0.1 in.	26
11.	Calculated Tip Breakdown Compared with Experimental Data for Frequency = 1500 MHz and Gap Height = 0.1 in.	27
12.	Calculated Tip Breakdown Compared with Experimental Data for Frequency = 1560 MHz and Gap Height = 0.2 in.	28
13.	Calculated Gap Breakdown Compared with Experimental Data for Frequency = 1560 MHz and Gap Height = 0.2 in.	30

I. INTRODUCTION

An important consideration in the design of microwave communications systems for reentry vehicles is the prediction of the radiated power levels at which the high-temperature gas surrounding the vehicle undergoes electrical breakdown. Several ingredients are necessary to make such a prediction: first, details of the flow-field mass density, species concentrations, and temperatures as functions of altitude must be available; second, the peak value of the spatial distribution of the electric field generated by the particular antenna considered must be known; and third, an analysis must be available for predicting voltage breakdown in the presence of electric-field and gas-property nonuniformities.

Our concern here is not with flow-field determination. We will concentrate on the determination of the electric field in a realistic geometry and will discuss the breakdown analysis for cold air. Specifically, we will study a sharp-nosed conical reentry vehicle with a symmetrical circumferential gap antenna that is excited at a frequency such that the vehicle length is approximately one wavelength long. This model is typical for small reentry vehicles operating in the VHF regime.

For this particular model, breakdown can occur both in the nose-tip region and in the vicinity of the feed gap. The electric field is, therefore, computed as a function of distance radially from the nose tip and as a function of distance normally from the feed gap. This calculation is accomplished first by the use of moment methods to obtain the current distribution on the vehicle

surface and then by the numerical integration of this current to obtain the electric field at any specified point in space. The current distribution calculation is closely related to previous work by Mautz and Harrington [1] and some earlier work by Andreassen [2].

Recently, several analyses [3]-[5] have become available for predicting microwave breakdown in the presence of nonuniformities. Epstein gave a variational technique that accommodates cw [5] or pulsed [6] breakdown and gas nonuniformities as well as electric-field nonuniformities. We will use this analysis with some modifications for the calculations.

Since all previous antenna breakdown calculations that account for nonuniformities have been confined to the case of a slot on an infinite ground-plane geometry [7], our major contribution in this paper is demonstrating that breakdown on a geometry that must be considered finite by virtue of its size relative to wavelength can also be predicted by existing techniques and models.

II. DESCRIPTION OF EXPERIMENTAL MODEL

The conical vehicle for which breakdown measurements were taken is shown in Fig. 1. The vehicle is split electrically to form an asymmetrical dipole with roll-symmetric excitation. The antenna is fed through a 50-ohm coaxial transmission line with a center conductor designed to provide a reflectionless transition to the radial transmission. The radial transmission line in turn excites the aperture.

The model was fabricated to the dimensions shown ± 0.001 in. The dimensions expressed in terms of wavelengths are consistent with an operating frequency of 1500 MHz. The assembly was sealed at one atmospheric pressure by machining tight-fitting dielectric in the feed line and at the aperture and by wetting the dielectric with silicone vacuum grease. After the antenna was fully assembled, a fine machine cut was taken along the cone to ensure that the dielectric window was flush with the aluminum body.

EFFICIENCY: $\approx 100\%$
VSWR AT INPUT: $< 2:1$

0.062
SPHERICAL R

ENLARGED VIEW A

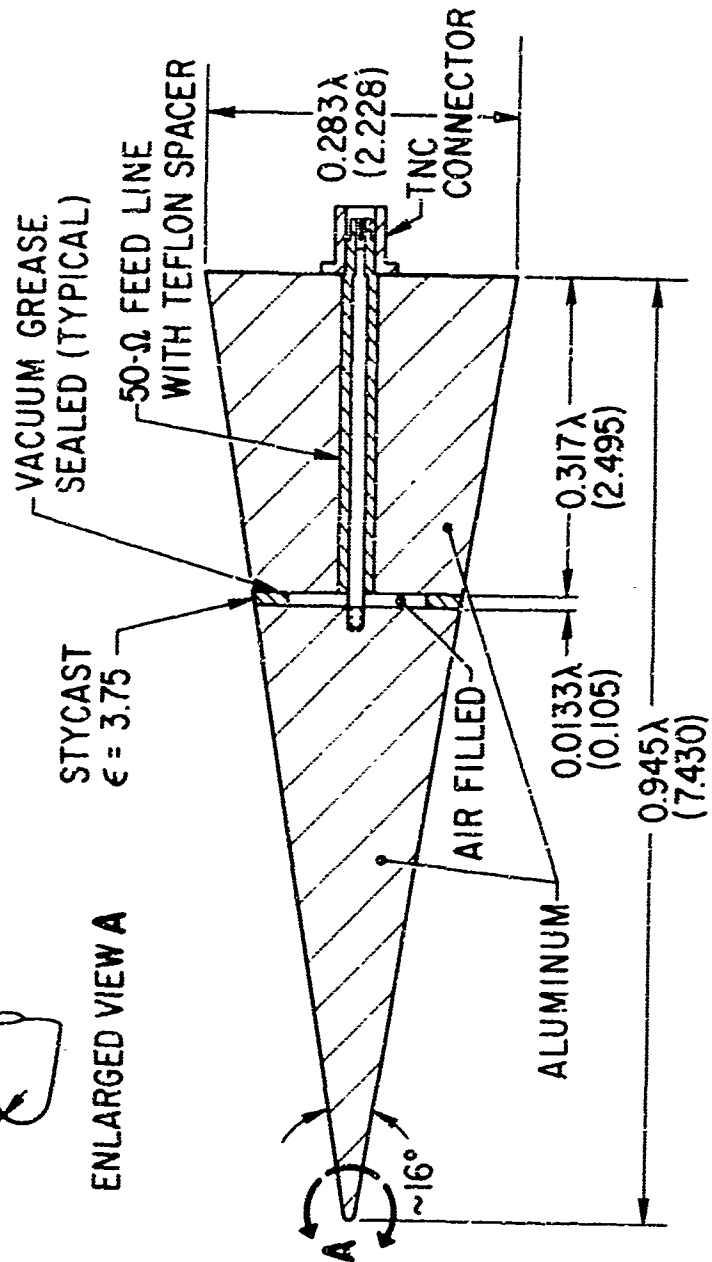


Figure 1. Model Circumferential Gap Antenna

III. NEAR-FIELD CALCULATIONS

The theoretical model is a figure of revolution with a generating curve that is a continuous function consisting of a circular arc representing the nose tip and two straight lines representing the sides and base of the cone (Fig. 2). The slight differences between this simplified geometry and the actual model are not important. The generating curve can be represented by a single variable t , and if a voltage V is applied across the feed gap, the tangential electric field on the surface of this vehicle can be assumed to be

$$\begin{aligned}\vec{E}_t &= \vec{a}_t \frac{V}{d} && (\text{at } t_1 \leq t \leq t_2) \\ \vec{E}_t &= 0 && (\text{elsewhere})\end{aligned}\tag{1}$$

where d is the gap width and \vec{a}_t is a unit vector tangent to the generating curve. The boundary condition that uniquely defines the exterior field configuration is represented by Eq. (1).

Complete details of the electric-field calculation are included elsewhere,^{*} therefore, this discussion will be brief. The problem was originally considered by Mautz and Harrington [1], who used moment methods to obtain the current distribution on the surface of the vehicle. The important differences between the present calculation and that of Mautz and Harrington will be brought out later in the discussion.

Essentially, moment methods include reducing an integral equation involving the unknown surface current (per unit width) \vec{J} to a set of linear algebraic equations of the form

^{*}K. M. SooHoo, "The Near and Far Fields of a Symmetrically Excited Finite Cone," to be published.

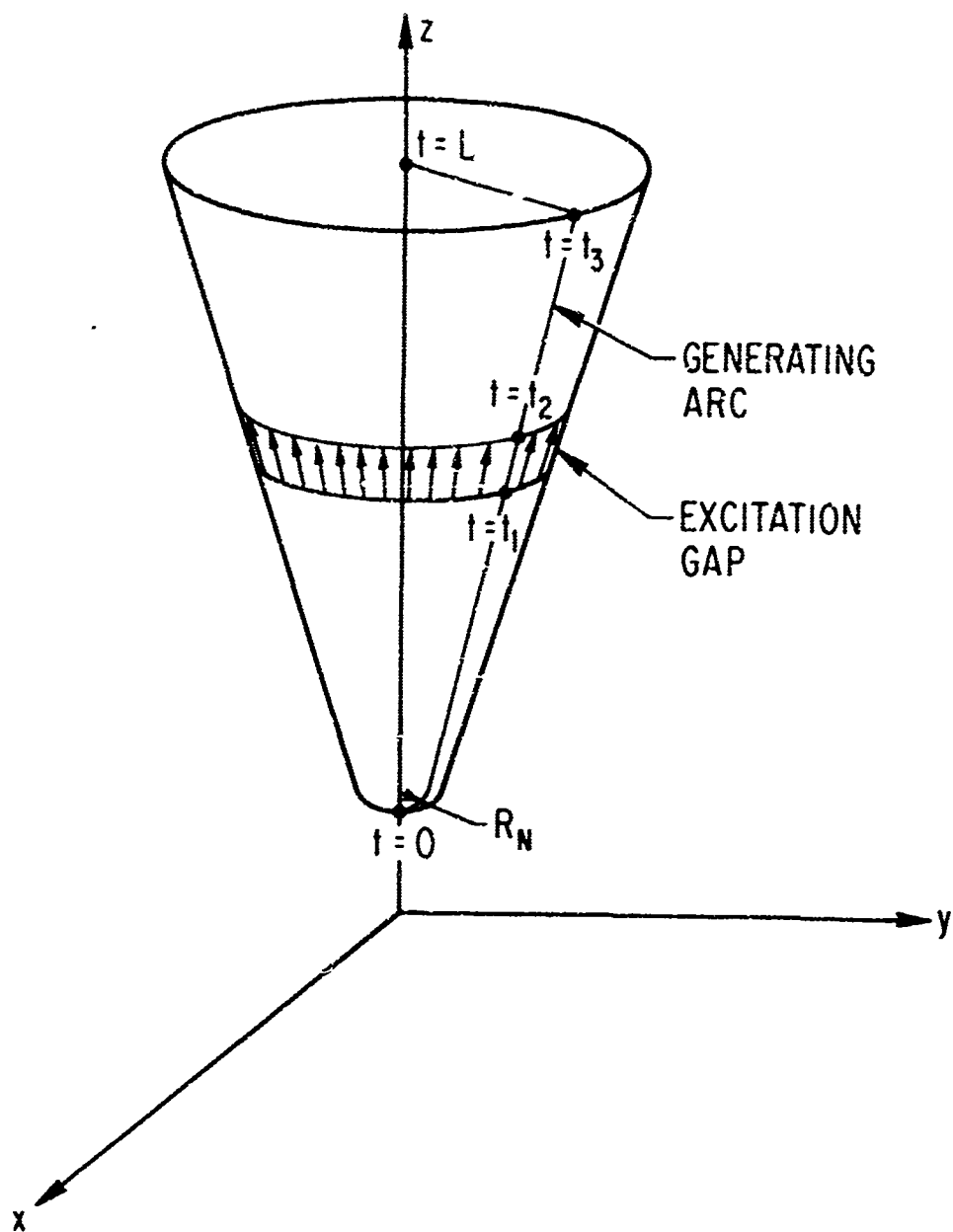


Figure 2. Theoretical Cone Model

$$[Z_{ij}][I_j] = [V_i] \quad (2)$$

which may then be solved for $[I_j]$ by standard matrix-inversion techniques. The column matrix $[V_i]$ is directly related to the given excitation or, in this case, Eq. (1). The symmetric matrix $[Z_{ij}]$ is a generalized impedance matrix with its elements dependent only on the geometrical configuration. Details of the calculation of $[Z_{ij}]$ and $[V_i]$ are given elsewhere.*

The relationship between \vec{J} and the elements of the column matrix $[I_j]$ is the finite sum

$$\vec{J}(t) = \sum_j I_j \vec{J}_j(t) \quad (3)$$

where \vec{J}_j are expansion functions that must be suitably chosen such that the elements of $[Z_{ij}]$ are relatively easy to compute, while, at the same time, Eq. (3) has reasonably good convergence.

The triangular expansion function suggested by Mautz and Harrington gives a piecewise-linear approximation to the current distribution. Here, triangular functions are also used; however, the exact form is different for the following reasons: First, the triangles are allowed to span unequal intervals so that a very accurate calculation of the current can be made on certain portions of the vehicle (e.g., where the near fields are of interest) without having to force the number of elements in $[Z_{ij}]$ to become excessively large. Second, Mautz and Harrington's expansion functions were actually the triangular function divided by the radial variable in cylindrical coordinates ρ .

*K. M. SooHoo, "The Near and Far Fields of a Symmetrically Excited Finite Cone," to be published.

This simplifies the calculations. However, it can be shown by the use of the continuity equation that ρ must be removed or the surface charge density becomes infinite whenever ρ goes to zero (e.g., the nose tip). Thus, in order to ensure that the correct normal electric field is computed at the nose tip, the expansion functions are chosen to be equal to the triangular function.

Calculations were made on a CDC 6600 computer. The total current $2\pi\rho(\vec{a}_t \cdot \vec{J}_t)$, as a function of distance along the generating curve, is shown in Fig. 3. The excitation for this case was 1 volt applied across a 0.1-in. gap. Sixty piecewise-linear intervals were used in this calculation.

Since the applied voltage is 1 volt, the computed current at the gap is also the input admittance. Thus, it can be seen that $Y_{in} = 0.009 + j \cdot 024$ mhos. Furthermore, since the total power radiated is the applied voltage squared times the input conductance, for an applied voltage of 1 volt, the total power radiated is 0.009 watts. This relationship is an important factor in computing the breakdown power curves.

The total power radiated (0.009 watts) was also obtained by integrating the Poynting vector over a far-field sphere. A measured directivity pattern, compared to the calculated pattern in which the current distribution of Fig. 3 is used, is shown in Fig. 4. The asymmetries in the measured pattern are an indication of its inaccuracies. Agreement, generally, is quite good.

Details of the near-field calculation are also given elsewhere.* The required integrations are performed in essentially the same manner as was involved in computing the elements of the generalized impedance matrix $[Z_{ij}]$. As mentioned earlier, the accuracy of this calculation is not critically tied to computer

*K. M. SooHoo, "The Near and Far Fields of a Symmetrically Excited Finite Cone," to be published.

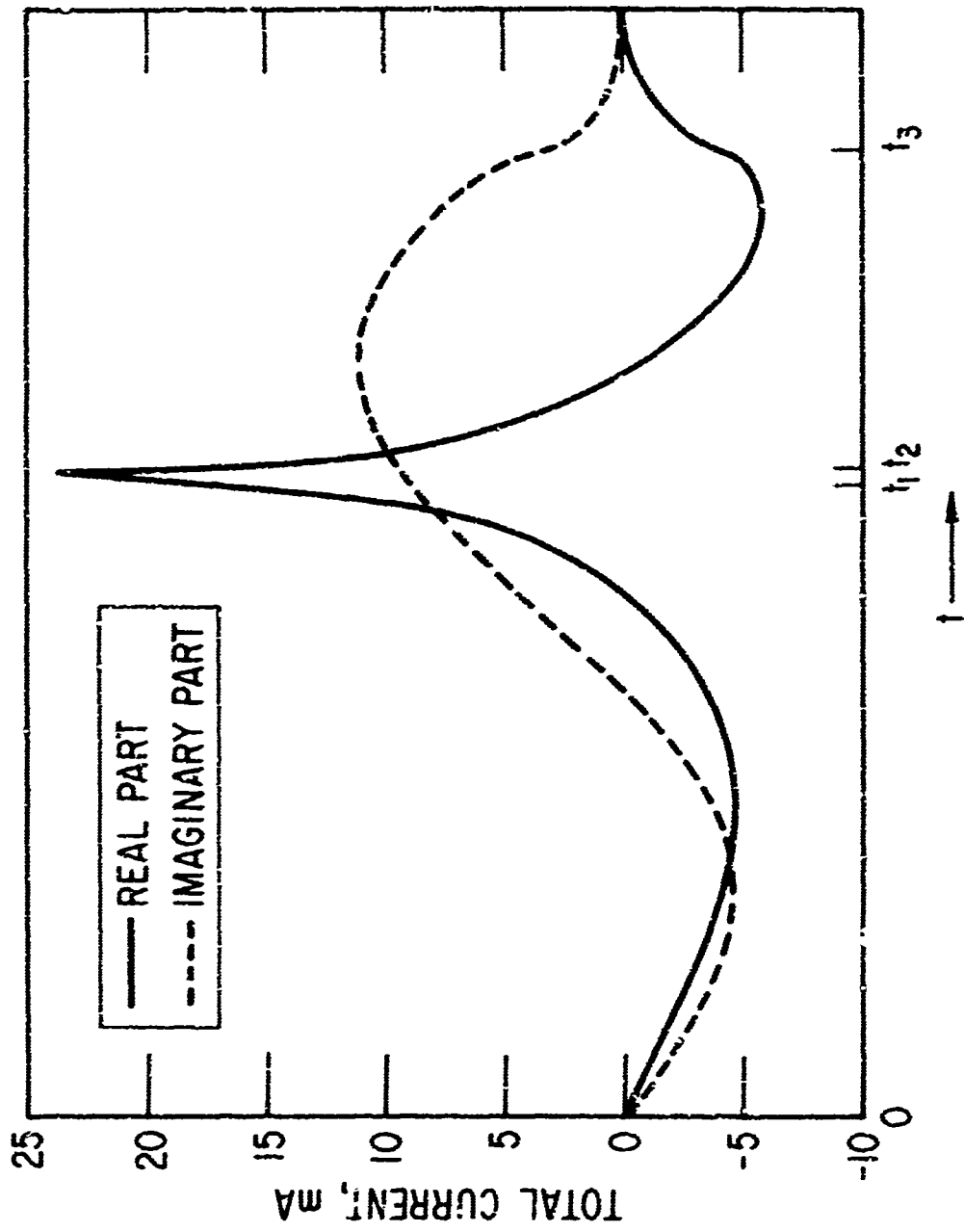


Figure 3. Total Current Distribution Along Generating Arc

time or computer storage, because it is only necessary to obtain a very accurate description of the current in the vicinity of the point at which the electric field is to be computed.

Figures 5 and 6 contain the required input data for the breakdown calculations described in the next section. Figure 5 shows the electric field as a function of distance from both the tip and feed gap, where the gap width is 0.1 in. and the frequency is 1500 MHz. Tip and gap field distributions, for a gap width of 0.2 in. at 1560 MHz are shown in Fig. 6.

The current distributions for the gap field calculations were approximated by 76 piecewise-linear intervals, where the 24 intervals in the vicinity of the gap were only one-third the size of the remaining 52 intervals. The current distributions for the tip field calculations were approximated by 81 piecewise-linear intervals, where the first eight intervals at the nose tip were one-fourth the size of the next 16, which, in turn, were one-sixth the size of the remaining 57 intervals. The near fields computed in this manner are estimated to have better than 5% accuracy.

These results are quite reasonable for the following reasons: First, at small distances from the vehicle surface, one expects the vehicle to appear as an infinite ground plane. Indeed, it was found that there are practically no differences between the gap fields shown in Figs. 5 and 6 and the calculated near field of an infinite ground plane [8]. Second, it can be seen that the tip fields appear to fall off inversely with distance. This is quite reasonable, since in this region the main contribution to the electric field is expected to come from a spherical wave originating at the nose tip as in

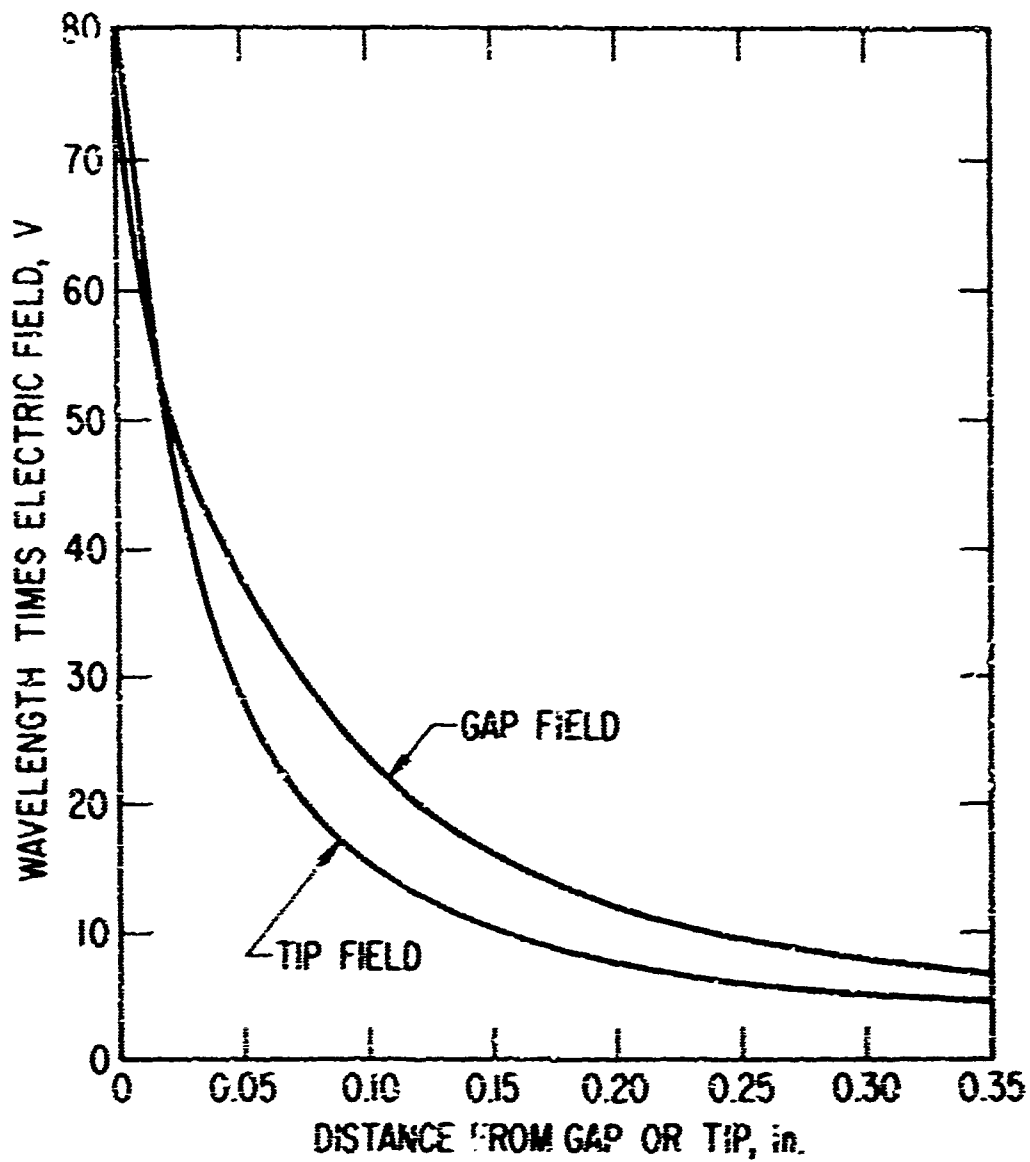


Figure 5. Near-Field Distributions at Gap and Tip for Frequency = 1500 MHz and Gap Height = 0.1 in.

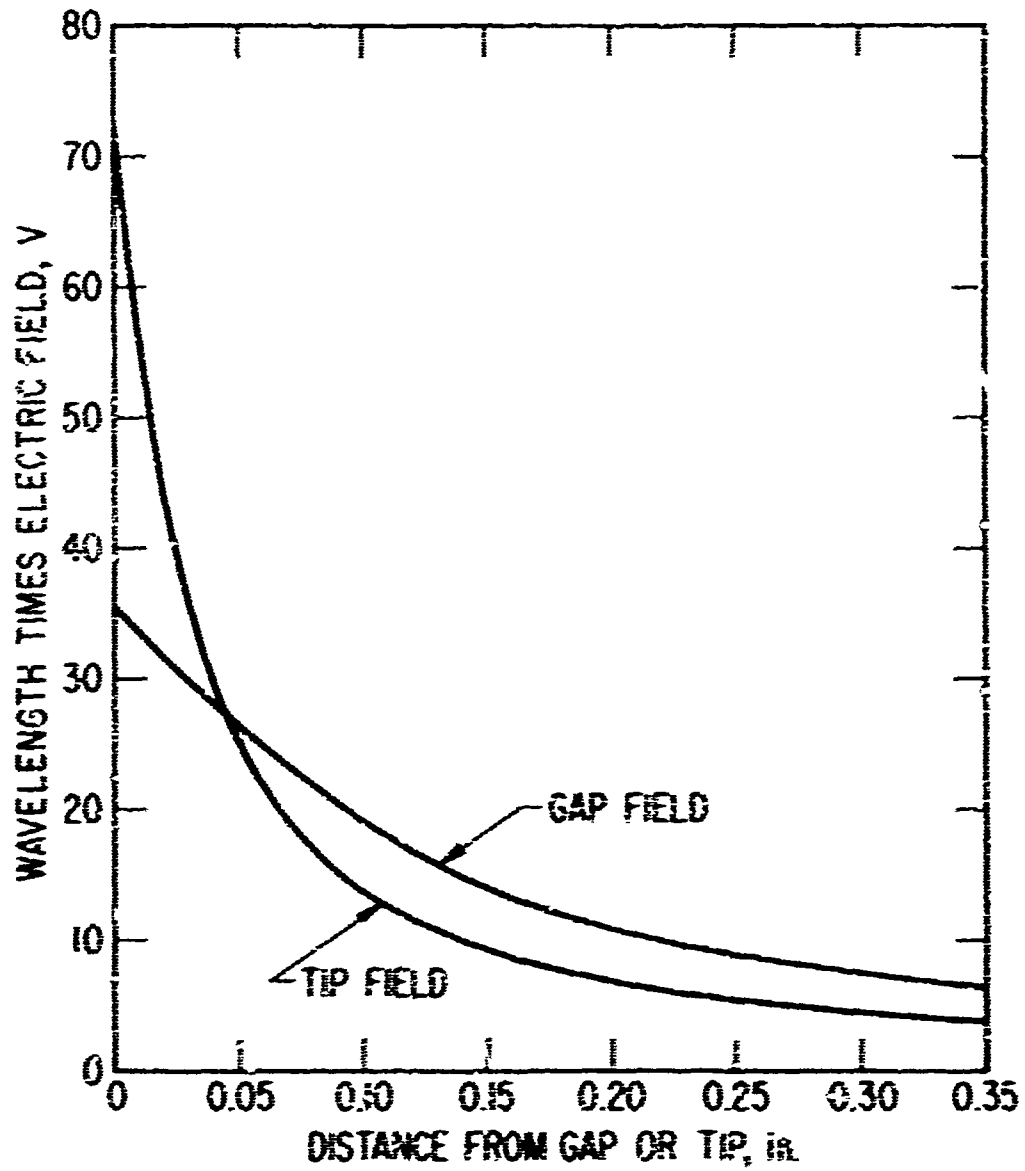


Figure 6. Near-Field Distributions at Gap and Tip for Frequency = 1560 MHz and Gap Height = 0.2 in.

the case of a thin, linear antenna [9]. At greater distances (at approximately 4 in. from the nose tip), as expected, the field begins to fall off inversely with distance squared.

IV. BREAKDOWN CALCULATIONS

The calculation of microwave breakdown in gases is based on the electron continuity equation of which we will adopt the following form

$$\frac{\partial n}{\partial t} = (\nu_i - \nu_a)n + \nabla \cdot (D\nabla n) \quad (4)$$

where n is the electron density. If the electric field is nonuniform, then the ionization frequency ν_i , the attachment frequency ν_a , and the diffusion coefficient D will vary spatially, since they are all functions of electric field. However, in cases where the electric field and gas properties are both uniform in space and time, these parameters are likewise independent of space and time. Then, by separation of variables, this equation can be integrated to yield

$$\frac{\ln(n/n_i)}{t} = (\nu_i - \nu_a) - \frac{D}{\Lambda^2} \quad (5)$$

where Λ is the characteristic diffusion length of the container or region in which breakdown is to be obtained and n_i is the initial electron density. For rectangular containers in which one dimension l is smaller than the others and, hence, dominates the determining diffusion losses, the characteristic diffusion length is $\Lambda = l/\pi$.

For cw breakdown one lets time t in Eq. (5) go to infinity or $\partial n/\partial t$ in Eq. (4) go to zero. The corresponding equations then are

$$\nu n + \nabla \cdot D\nabla n = 0 \quad (6)$$

and

$$\nu - \frac{D}{\Lambda^2} = 0 \quad (7)$$

where we now define $\nu \equiv \nu_i - \nu_a$.

In the experiment reported here, it is expected that the pulse duration of the microwave power is sufficiently long that the condition of cw breakdown, as opposed to pulsed breakdown, is achieved. It will be seen that the analysis to be described for breakdown in a nonuniform field will yield a value for the effective diffusion length Λ_e . This allows us through the use of terms in Eq. (5) to determine approximately the validity of the assumption that cw breakdown conditions have been realized in the experiment. We place the calculated value of Λ_e and the value of pulse duration τ_b used in the experiment into the following relation

$$R = \frac{\Lambda_e^2 \ln(n_b/n_i)}{D\tau_b} \quad (8)$$

which expresses the ratio of finite time effects to diffusion effects in determining the breakdown level. In Eq. (8), n_b is the electron density that defines breakdown and is usually taken to be the critical electron density. If $R \ll 1$, cw breakdown conditions apply, and the use of a cw breakdown analysis is appropriate. This quantity will be evaluated systematically with the calculated values of Λ_e .

For a nonuniform electric field Epstein has given a variational analysis that we will use. This analysis is discussed in greater detail in [10] and is

briefly outlined below. His analysis shows that Eq. (6) can be expressed as a variational statement

$$\delta \int_0^1 [\lambda n^2 - g(\nabla n)^2] d\xi = 0 \quad (9)$$

where we consider only one dimension and introduce the following dimensionless parameters: $f(\xi) \equiv v(\xi)/v_0$, $g(\xi) \equiv D(\xi)/D_0$, $\lambda \equiv v_0 \ell^2 / D_0$, and $\xi \equiv x/\ell$, where the subscript zero denotes a convenient reference point, usually the point of maximum field strength. A Ritz method is then used to solve this equation. We use a trial function of two undetermined constants that meets the boundary conditions on electron density

$$n = C_1 \xi(1 - \xi) + C_2 \xi(1 - \xi)^k \quad (10)$$

This trial function is inserted into Eq. (9) and the result is a quadratic equation for λ , where the smallest positive root is the breakdown solution.

For the functional dependence of the various parameters, we have used [11] to obtain v/p vs E_e/p , [12] to obtain $Dp = (29 + 0.9 E_e/p) \times 10^4$ $\text{cm}^2\text{-torr/sec}$, and [14] to obtain $\bar{v}_c/p = 5.3 \times 10^9 \text{ sec}^{-1} \text{ torr}^{-1}$.

These relationships are such that $f(\xi)$ and $g(\xi)$ depend on the magnitude of the field as well as its distribution in space. Epstein, therefore, proposed to iterate on this procedure until a consistent solution is found. We depart from Epstein's method at this point and take advantage of the fact that we are considering only uniform gas properties. If we note that the functions v/p and Dp can be expressed as functions of E_e/p only, for $p/\omega < 10^{-8}/6\pi \text{ Torr-sec}$ [13],

it is clear that $f(\xi)$ and $g(\xi)$ are unique functions of $E_e(\xi)/p$ also. Then, if we assume a collision frequency that depends only on gas pressure, i. e., $\bar{\nu}_c/p = \text{constant}$, $E_e(\xi)/p$ is a function of electric field and gas pressure

$$\frac{E_e(\xi)}{p} = \frac{E_{rms}(\xi)}{\left[p^2 + \left[\omega / \bar{\nu}_c / p \right]^2 \right]^{1/2}} \quad (11)$$

For a uniform, but for the time being arbitrary, gas pressure the spatial variation of $E_e(\xi)/p$ is just that of $E_{rms}(\xi)$. If we specify the value of (E_e/p) , then for a known E-field distribution, $f(\xi)$ and $g(\xi)$ are determined.

Once λ is found from Eq. (9), we can find the pressure for which the solution is valid, i. e.,

$$p = \left[\lambda (D_o p) \left(\frac{p}{v_o} \right) \left(\frac{1}{l^2} \right) \right]^{1/2} \quad (12)$$

and the corresponding electric field $(E_{rms})_o$ can be found from Eq. (11). It is also possible to find an effective diffusion length, i. e.,

$$\Lambda_e^2 = \frac{D_o}{v_o} = \frac{l^2}{\lambda} \quad (13)$$

One can then run through successive values of $(E_e/p)_o$ and find values of pressure and electric field for breakdown for each value.

The question arises as to what values of the integration interval l and of the exponent k in Eq. (10) to chose. It can be shown that this analysis leads to an approximate eigenvalue λ that is an upper bound to the true value and also

that it is a property of the analysis that the solution is stationary with respect to the trial function. However, it is possible to improve on the estimated breakdown field by repeating the calculation for several values of k and l . The best solution is the lowest eigenvalue at any given pressure for all combinations of k and l . Accordingly, the values of k and l used in the calculations reported here were varied successively and systematically until minimum eigenvalues were found.

The electric-field distributions depicted in Figs. 5 and 6 were used to perform the preceding breakdown calculations. The resulting values of Λ_e and R are plotted in Figs. 7 and 8. In evaluating R , we have used $(n_b/n_0) = 10^9$, $\tau_b = 10$ microseconds, and D evaluated at peak field, i. e., $D = D_0$. Clearly, the conditions of cw breakdown were satisfied in this experiment. The important results of these calculations, i. e., plots of incident power for breakdown versus pressure, are shown in Section V along with the experimental data.

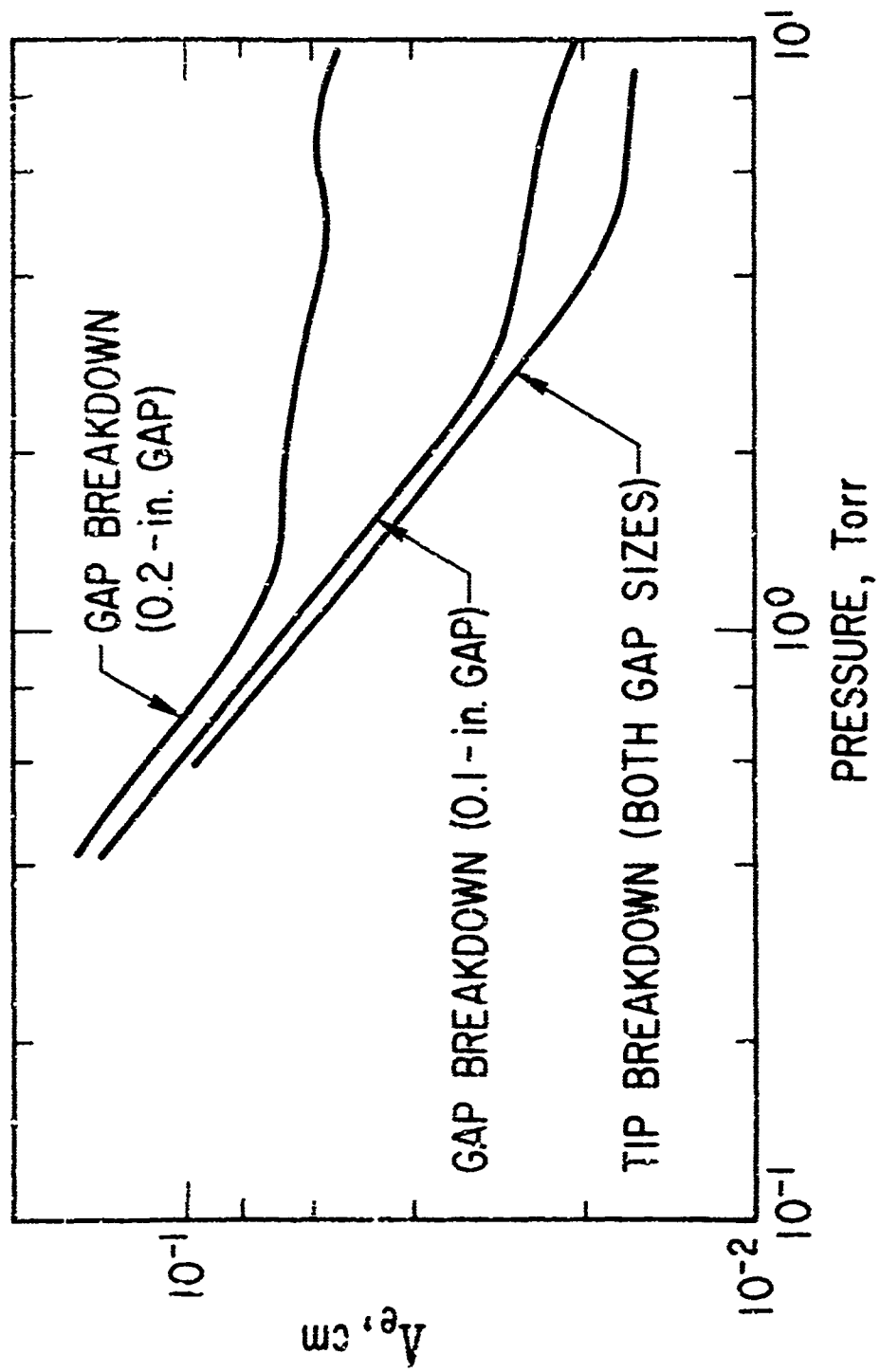


Figure 7. Calculated Diffusion Length A_e

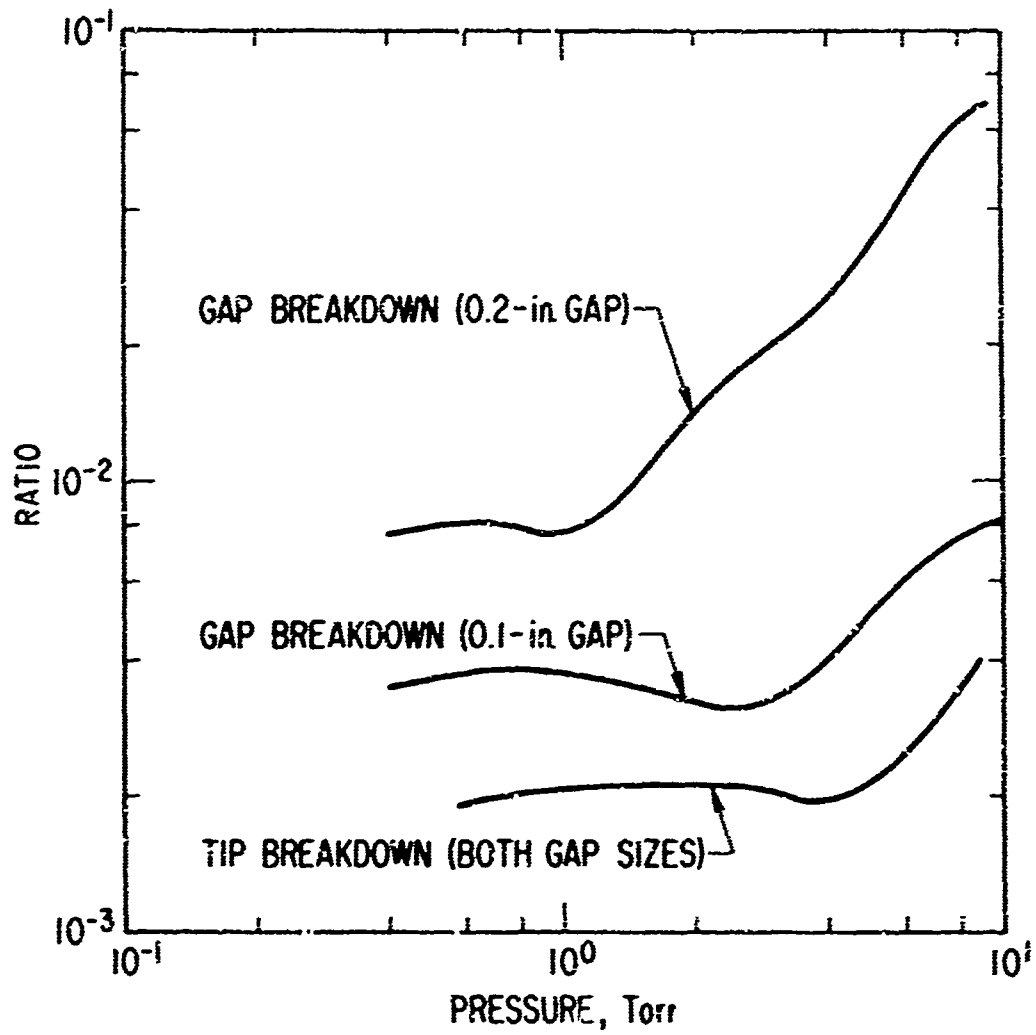


Figure 8. Test for Validity of CW Breakdown Assumption
Ratio of Finite Time to Diffusion Time

V. EXPERIMENT AND RESULTS

The breakdown test apparatus consists of a high-power RF source, an RF transparent vacuum chamber in which the antenna under test was placed, and the set of sensing instrumentation and visual display (Fig. 9). The vacuum chamber is a 5-foot diameter plexiglass sphere with 0.5-in. thick walls. A low-level radioactive source was placed in the chamber near the antenna to provide a few free electrons from which the breakdown avalanche could start when critical power was applied. All cables and directional couplers that lead to meter readouts and to the antenna were calibrated as a system so that the interaction of component mismatches could be included in the calibration.

The VSWR and efficiency of the antenna was determined on a network analyzer prior to breakdown testing. Then, the VSWR was again measured while the antenna was in the vacuum chamber by the use of the forward- and reflected-power meters shown in Fig. 9. This served as a secondary check on the cabling system and antenna after all test apparatus was in place and connected.

With the vacuum chamber pressure fixed, the variable attenuator was used to increase the power applied to the antenna until antenna breakdown occurred. Breakdown was always observed visually at the antenna aperture and by a corresponding increase in reflected power as observed on the reflected power meter and the dual-trace oscilloscope. The forward power (less the reflected power) at incipient breakdown, corrected for both cable and directional coupler losses, was recorded as the breakdown power. This process was

PRECEDING PAGE BLANK

repeated for each air pressure. The antenna feed network including the radial line terminating in the circumferential gap was sealed at one atmosphere, because it was found that internal arcing would occur at low air pressure. The applied power was pulsed at 1000 cycles per second, and the pulses were 10 microseconds wide. The pulse rate was varied extensively, and breakdown threshold was found to be independent of pulse rate.

Measured breakdown power along with the computed results for the 0.1-in. gap are shown as functions of pressure on Figs. 10 and 11. As indicated, feed-gap breakdown was observed at pressures below 1.0 Torr, while at pressures above 2.9 Torr, breakdown occurred at the nose tip. In this latter regime, subsequent gap breakdown could be attained by a further increase of the incident power. However, this data is not shown, since it is not known how tip breakdown should influence the near-field calculation at the gap.

In the region between 1.0 and 2.9 Torr, it appeared that breakdown was initiated simultaneously in both tip and gap regions. However, an apparent discontinuity exhibited by the data at 1.8 Torr indicates that the crossover from gap to tip breakdown actually occurred at that point. Thus, on Fig. 10 the calculated and measured curves should be compared only up to 1.8 Torr, while on Fig. 11 comparisons should only be made at pressures above 1.8 Torr.

The gap width was extended to 0.2 in. in order to avoid the problem of overlapping breakdown regions. For this case, tip breakdown occurred at all the levels of pressure tested. The comparison between theory and measurement is shown in Fig. 12. The operating frequency for this case was changed to 1560 MHz. In order to preclude tip breakdown, the nose tip was covered with dielectric.

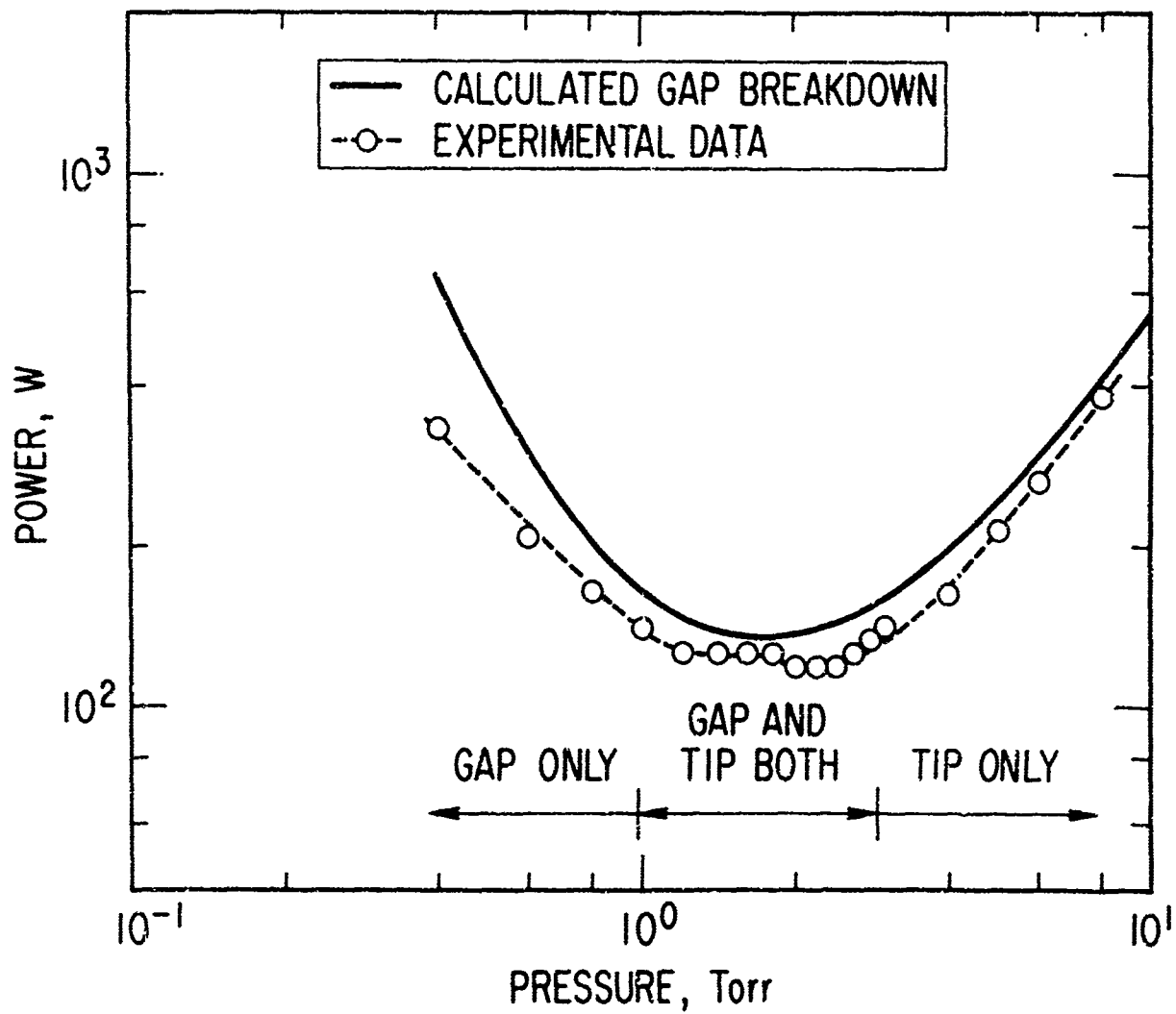


Figure 10. Calculated Gap Breakdown Compared with Experimental Data for Frequency = 1500 MHz and Gap Height = 0.1 in.

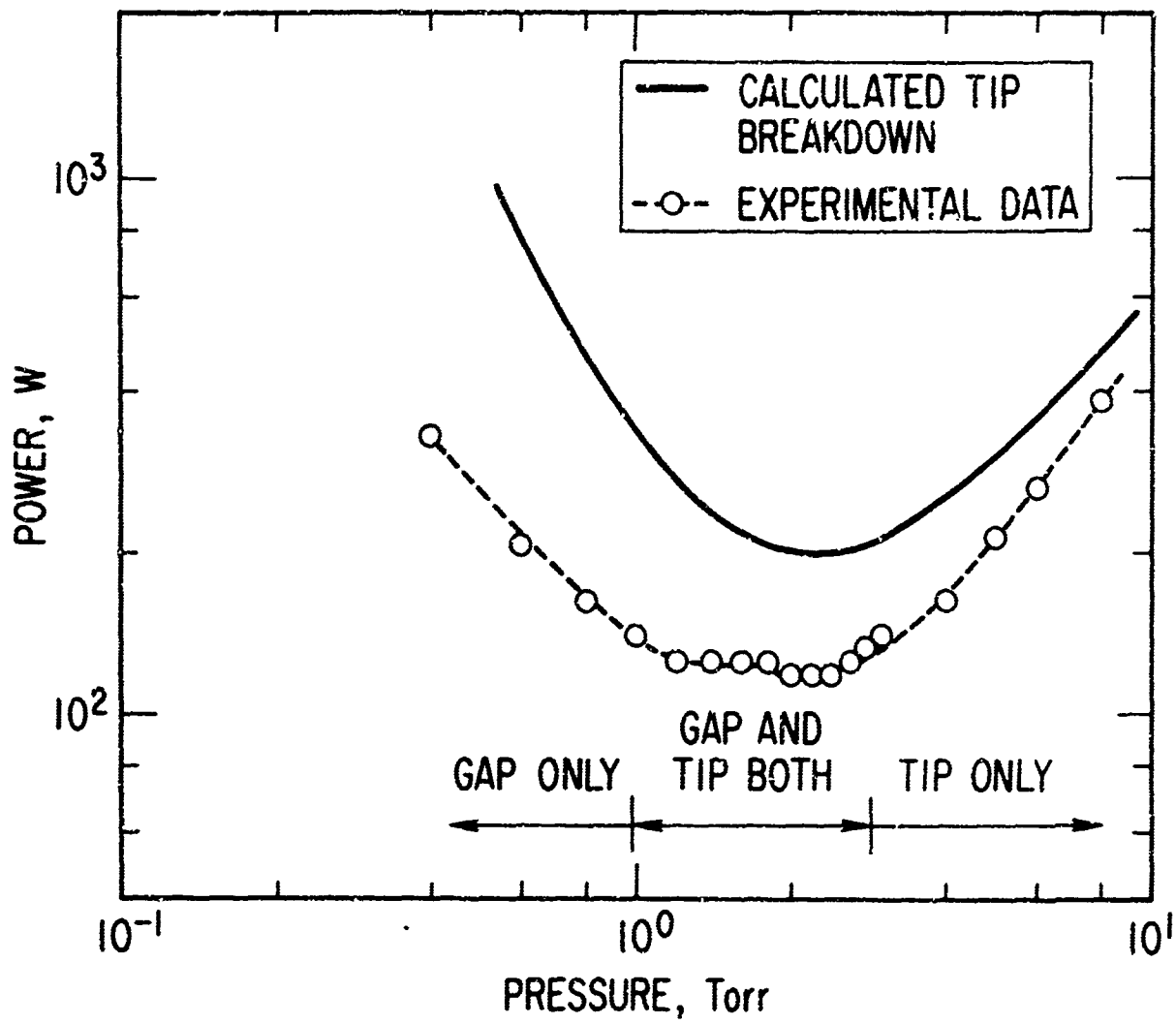


Figure 11. Calculated Tip Breakdown Compared with Experimental Data for Frequency = 1500 MHz and Gap Height = 0.1 in.

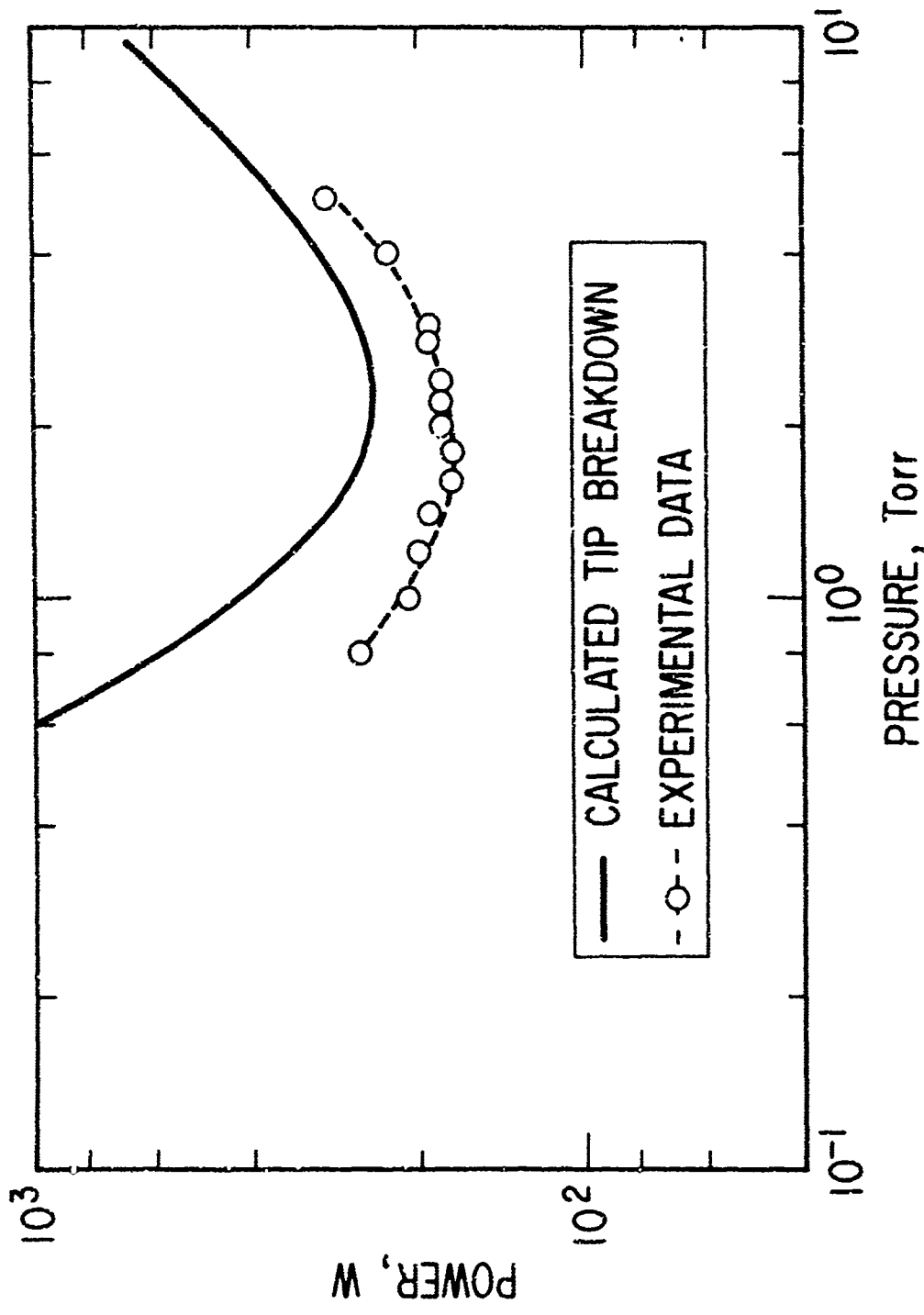


Figure 12. Calculated Tip Breakdown Compared with Experimental Data for Frequency = 1560 MHz and Gap Height = 0.2 in.

The resultant gap breakdown data along with the computed curve is shown in Fig. 13. The effect of a dielectric covered tip was not included in the calculations.

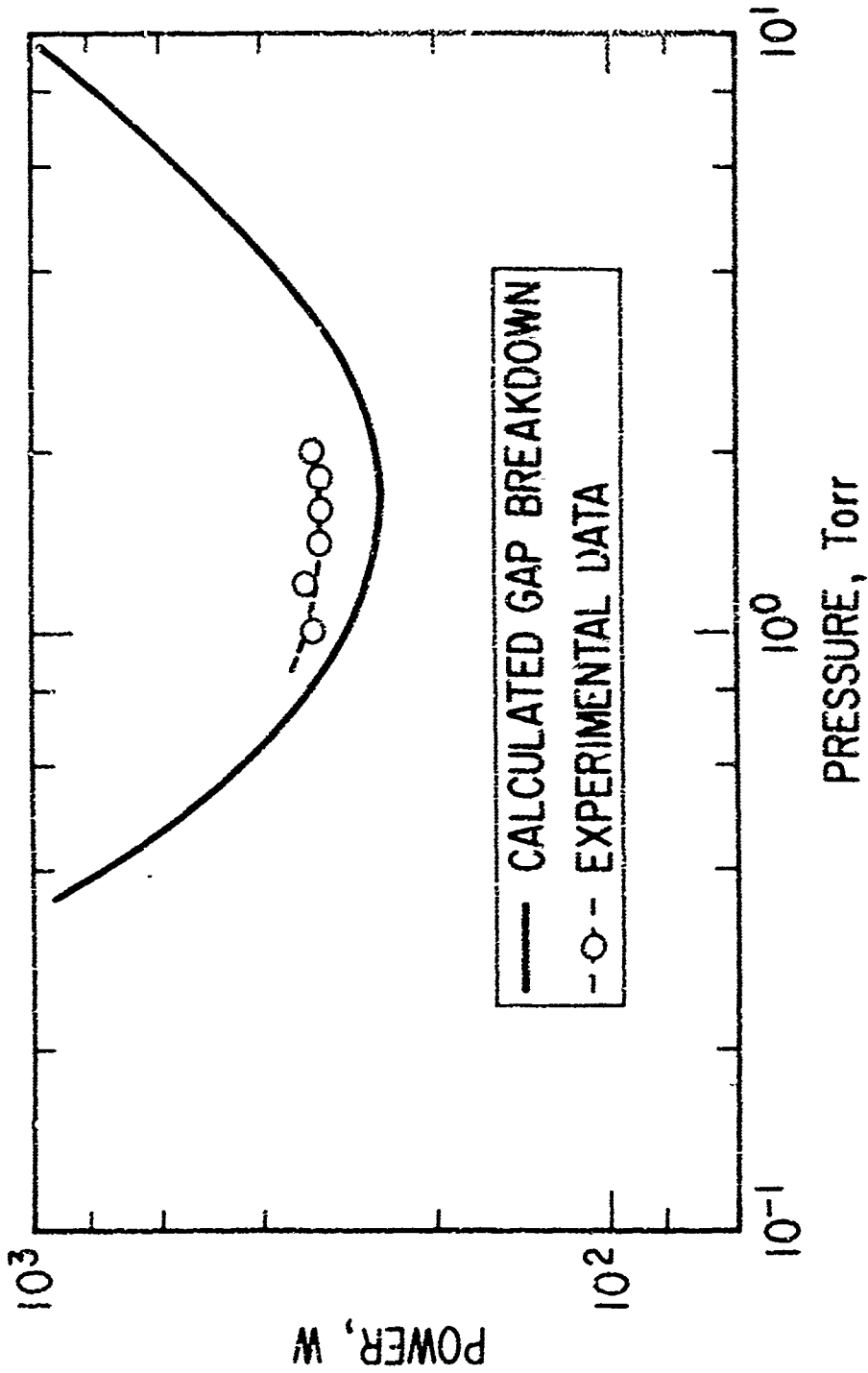


Figure 13. Calculated Gap Breakdown Compared with Experimental Data for Frequency = 1560 MHz and Gap Height = 0.2 in.

VI. DISCUSSION

Instrumentation and reading inaccuracies and errors associated with estimating internal system losses (efficiency) are the principal contributors to errors in the measured data. In addition, the electric-field distributions may have been distorted to some degree by the plexiglass chamber walls and by the presence of the feed cable. These latter two effects were not, however, found to be significant. A crude estimate of the overall accuracy of the breakdown data is ± 1.5 dB.

It can be seen from Figs. 10 and 13 that the calculated and measured gap breakdown curves are in agreement within the estimated accuracy of the data. For tip breakdown, agreement is not as good, but, for the most part, it is still within the accuracy of the data.

It is, therefore, concluded that the breakdown power levels for a symmetrically excited finite body can be predicted with sophisticated numerical techniques and a high-speed digital computer. The better agreement exhibited by gap breakdown may be attributed to the fact that the breakdown model only accounts for one-dimensional nonuniformities, and the electric-field fall-off behavior at the gap is obviously more one dimensional than at the tip.

REFERENCES

- [1] J. R. Mautz and R. F. Harrington, "Radiation and scattering from bodies of revolution," Appl. Sci. Res., vol. 20, pp. 405-435, June 1969.
- [2] M. G. Andreassen, "Scattering from bodies of revolution," IEEE, Trans. on Antennas and Propagation, vol. AP-13, pp. 303-310, March 1965.
- [3] J. T. Mayhan and R. L. Fante, "A variational formulation specifying the breakdown criteria for plasmas subjected to spatially nonuniform electric fields," J. Appl. Phys., vol. 40, No. 2, pp. 449-453, February 1969.
- [4] J. T. Mayhan and R. L. Fante, "Microwave breakdown over a semi-infinite interval," J. Appl. Phys., vol. 40, No. 13, pp. 5207-5211, December 1969.
- [5] M. Epstein, "High frequency breakdown on nonuniform gases in spatially varying fields," Phys. Fluids, vol. 11, No. 4, pp. 896-902, 1968.
- [6] M. Epstein, "Pulsed breakdown in nonuniform fields," Phys. Fluids, vol. 12, No. 3, pp. 728-729, March 1969.
- [7] G. C. Light, "The effects of spatial nonuniformities on high temperature microwave breakdown," Proc. of the Ninth Plasma Sheath Sym., October 13-15, 1970, NASA Langley Research Center, Hampton, Va. Also, TR-0059(6220-10)-6, The Aerospace Corporation, El Segundo, Calif., 7 FEB 62.

PRECEDING PAGE BLANK

- [8] R. L. Fante and J. T. Mayhan, "Complete electric field of the infinite slot antenna," IEEE Trans. on Antennas and Propagation, vol. AP-17 p. 97, January 1969.
- [9] E. C. Jordan, Electromagnetic Waves and Radiating Systems, Englewood, Cliffs, New Jersey: Prentice-Hall, Inc., 1961, pp. 320-325.
- [10] G. C. Light, "Microwave breakdown in the presence of spatial nonuniformities: computer programs," TR-0059(6220-10)-4, The Aerospace Corporation, El Segundo, Calif., 70 SEP 30.
- [11] W. Scharfman and T. Morita, "Focused microwave technique for measurement of the ionization rate and collision frequency," J. Appl. Phys. vol. 35, No. 7, pp. 2016-2020, 1964.
- [12] A. D. MacDonald, D. V. Gaskell, and H. N. Gitterman, "Microwave breakdown in air, oxygen, and nitrogen," Phys. Rev., vol. 130, pp. 1841-1850, June 1963.
- [13] L. Gould and L. W. Roberts, "Breakdown of air at microwave frequencies," J. Appl. Phys., vol. 27, No. 10, pp. 1162-1170, 1956.